Proc. Natl. Acad. Sci. USA
Vol. 96, pp. 8829–8834, August 1999
Applied Physical Sciences, Physiology

Complexity of terminal airspace geometry assessed by lung computed tomography in normal subjects and patients with chronic obstructive pulmonary disease

MICHIAKI MISHIMA†, TOYOHIRO HIRAI‡, HARUMI ITOH§, YASUTAKA NAKANO‡, HIROAKI SAKAI‡, SHIGEO MURO‡, KOICHI NISHIMURA‡, YOSHITAKA OKU‡, KAZUO CHIN†, MOTOHARU OHI‡, TAKASHI NAKAMURA†, JASON H. T. BATES¶, ADRIANO M. ALENCAR‖, AND BÈLA SUKI‖,††

Departments of †Physical Therapeutics, ‡Pulmonary Medicine, and §Radiology, Kyoto University Hospital, Kyoto 606-8507, Japan; ¶Meakins-Christie Laboratories, McGill University, Montreal, Canada H2X 2P2; and ‖Department of Biomedical Engineering, Boston University, Boston, MA 02215

Communicated by Ewald R. Weibel, University of Bern, Herrenschwanden, Switzerland, June 3, 1999 (received for review September 1, 1998)

ABSTRACT **Increases in the low attenuation areas (LAA) of chest x-ray computed tomography images in patients with chronic obstructive pulmonary disease (COPD) have been reported to reflect the development of pathological emphysema. We examined the statistical properties of LAA clusters in COPD patients and in healthy subjects. In COPD patients, the percentage of the lung field occupied by LAAs (LAA%) ranged from 2.6 to 67.6. In contrast, LAA% was always <30% in healthy subjects. The cumulative size distribution of the LAA clusters followed a power law characterized by an exponent *D*. We show that *D* is a measure of the complexity of the terminal airspace geometry. The COPD patients with normal LAA% had significantly smaller *D* values than the healthy subjects, and the *D* values did not correlate with pulmonary function tests except for the diffusing capacity of the lung. We interpret these results by using a large elastic spring network model and find that the neighboring smaller LAA clusters tend to coalesce and form larger clusters as the weak elastic fibers separating them break under tension. This process leaves LAA% unchanged whereas it decreases the number of small clusters and increases the number of large clusters, which results in a reduction in *D* similar to that observed in early emphysema patients. These findings suggest that *D* is a sensitive and powerful parameter for the detection of the terminal airspace enlargement that occurs in early emphysema.**

High-resolution computed tomography (CT) is a sensitive and noninvasive tool for assessing alterations in lung structure induced by various disease processes. Increases in the low attenuation areas (LAA) in the lung regions of chest x-ray CT images in patients with chronic obstructive pulmonary disease (COPD) have been reported to reflect the development of pathological emphysema (1–4). Nevertheless, previous methods of analyzing lung CT images are limited for general clinical diagnostic purposes (5) because the size and spatial distribution of LAAs are not taken into account. Recently, Uppaluri *et al.* (6) found that a texture-based adaptive multiple feature method could differentiate between normal and emphysematous tissue with 100% accuracy. However, it is not clear whether this method would detect early emphysema. More recently, Shimizu *et al.* (7) proposed a promising fractal analysis method for assessing ground-glass opacities in lung CT images. Their approach was able to successfully differentiate between fibrotic and nonfibrotic disease processes.

The concept of fractal geometry was developed by Mandelbrot (8) to quantitatively describe the random variations in size and shape seen in natural objects. A fractal object is said to be scale-free because its characteristics are invariant under isotropic scale transformations. Such scale-invariance can be achieved if the object is formed by parts that are similar to the whole. In other words, fractals are self-similar and hence are characterized by power law functions (the only mathematical functions obeying scale-invariance) and a noninteger dimension d_f, called the fractal dimension. When the numerical value of d_f is close to the smallest integer $>d_f$, the dimension of the embedding space, the space filling capacity of the object approaches that of an Euclidean object. The methodology of characterizing fractals has been successfully applied to pulmonary physiology (9, 10). For example, Horsfield found fractal properties in the relationship between the generation number and mean diameter of airways in the bronchial tree (11). The perimeter of alveolar wall sections (12) and pulmonary blood flow (13, 14) also were reported to have fractal properties. Additionally, Gilliard *et al.* reported that surfactant administered transbronchially to rabbit lungs showed a fractal distribution (15). These studies suggest that many attributes of the lung have fractal properties.

The purpose of this present study is to examine the extent to which LAA clusters in both healthy subjects and COPD patients reveal the underlying fractal structure of the lung and to assess the usefulness of this approach in early detection of emphysema. Because the LAA clusters result from taking a slice through the alveolar fractal surface, we quantified the size distribution of the LAA clusters in healthy subjects and COPD patients. We also developed a structural model of a slice of lung tissue based on a network of interconnected springs. This model allowed us to investigate how destructive changes mimicking the pathogenesis of early emphysema can affect the size distribution of LAA clusters.

Size Distribution of LAA Clusters in CT Images

Seventy-three patients with COPD and thirty normal age-matched controls were studied. All subjects were male and were current or ex-smokers. The diagnosis of COPD was made on the basis of clinical symptoms, lung function tests, and plain chest roentogenographs (16). The x-ray CT scanning and lung function tests were performed on the same day. Bronchodilators were stopped 48 hours before the examination. Airflow limitation in the patients was defined as a FEV1/FVC (ratio of forced expiratory volume in 1 second to forced vital

The publication costs of this article were defrayed in part by page charge payment. This article must therefore be hereby marked "*advertisement*" in accordance with 18 U.S.C. §1734 solely to indicate this fact.

PNAS is available online at www.pnas.org.

Abbreviations: LAA, low attenuation areas; CT, computed tomography; COPD, chronic obstructive pulmonary disease; FEV1/FVC, ratio of forced expiratory volume in 1 second to forced vital capacity; DLCO/VA, ratio of diffusing capacity to alveolar ventilation.

††To whom reprint requests should be addressed at: Department of Biomedical Engineering, Boston University, 44 Cummington Street, Boston, MA 02215. E-mail: bsuki@bu.edu.

capacity) of <70%. The normal subjects had no respiratory symptoms and had normal lung function. The study protocol was approved by the ethics committee of Kyoto University, and written informed consent was obtained from each subject before the study. Conventional lung function testing was performed with a Chestac-65V (Chest, Kyoto). Lung volume was measured by the helium dilution method, and diffusing capacity was estimated by the carbon monoxide single breath method. All data were presented as mean and standard deviation (SD), and statistical comparisons between the normal and COPD groups were performed by using the Mann–Whitney *u* test. The age, FEV1/FVC, and the ratio of diffusing capacity to alveolar ventilation (DLCO/VA) in the normal and COPD groups were 63.9 ± 14.6 vs. 68.7 ± 6.2 years, 79.6 ± 6.8 vs. 35.2 ± 12.9% ($P < 0.0001$ compared with normal), and 4.90 ± 1.05 vs. 3.67 ± 1.14 ml/min/mmHg/l ($P < 0.0001$ compared with normal), respectively.

The CT scans were performed by using a high-resolution CT: X-Vigor (Toshiba, Tokyo) scanner with a 2-mm slice thickness, a scanning time of 1.0 seconds, a voltage of 120 kV, a current of 200 or 250 mA, and a field of view of 32 cm. All subjects were scanned in the supine position. During the scan, the subjects held their breath after a deep inspiration. This minimized the influence of air-trapping and allowed us to relate the results to diffusing capacity under the same conditions: i.e., after a deep inspiration. No contrast medium was used, and three slices (upper, middle, and lower lung) from each patient were analyzed (17). High-resolution CT images of 512 × 512 pixels (pixel dimension 0.0625 cm) were calculated by a standard reconstruction algorithm (FC85). The lung fields were automatically identified in each image as contiguous regions having Hounsfield units less than a specified threshold value (17, 18). We found that one SD below the mean Hounsfield units of the lungs from eight normal subjects who never smoked was −957 Hounsfield units, and we therefore identified the LAAs as those regions of contiguous pixels having Hounsfield units <−960. A comparison between the original and LAA image in a representative COPD subject is shown in Fig. 1 *A* and *B*. The values of LAA% from the COPD patients spanned a large range, from 2.6 to 67.6. In contrast, the LAA% of the normal subjects were all <30, and the range spanned by ± SD was 31.6. Thus, COPD patients can be classified into two groups: one with normal LAA% (<30) and the other with elevated LAA% (>30). We designate these two groups as COPD ≤ 30 and COPD > 30, respectively. The LAA images of a normal subject and a COPD ≤ 30 patient having similar LAA% (≈7%) are compared in Fig. 1 *C* and *D*, respectively. These images show that the COPD patient had fewer but somewhat larger clusters of LAAs than the normal subject.

Fig. 2 demonstrates that the cumulative frequency distributions of LAA sizes decrease linearly on a log-log plot. The slopes of the plots vary between subjects and as a function of LAA%, but, in each case, the cumulative frequency distribution, *Y*, can be described by a power law of size *X* of the form

$$Y = K^*X^{-D} \quad [1]$$

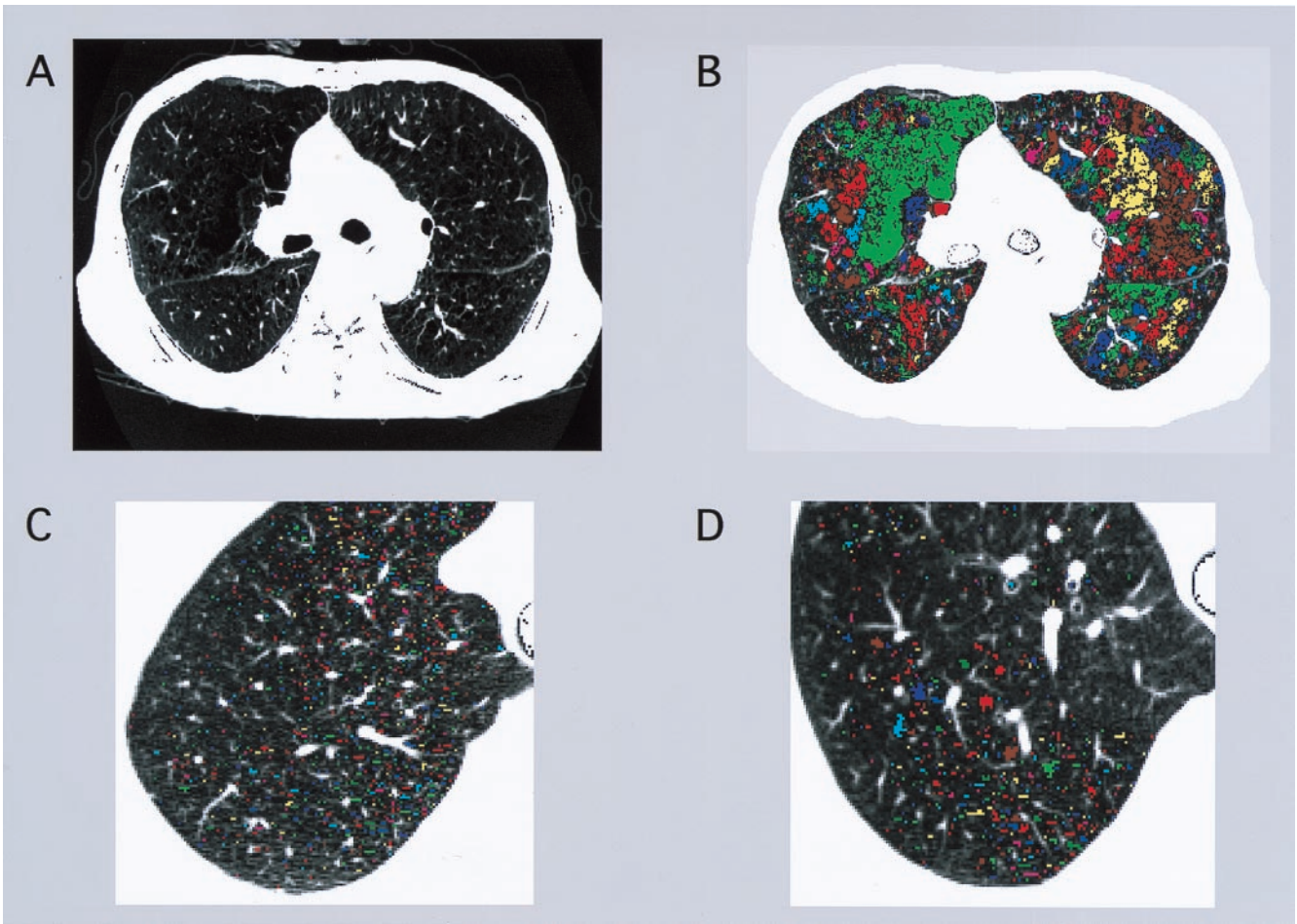

FIG. 1. (*A*) Original CT image of the middle lung slice in a representative COPD patient. LAA% is 55.1. (*B*) The same image as in *A*, but the individual clusters comprising contiguous LAA regions are shown in contrasting colors. The lung field was identified from the rest of the image, and the lumen of the trachea and large bronchi were excluded. The white regions are smaller airways and vessels. (*C*) LAA image of a normal subject. (*D*) LAA image of a COPD patient. The LAA% and exponent *D* of the cluster distribution of the two images in *C* and *D* are 7.2 vs. 7.1 and 2.97 vs. 1.71, respectively.

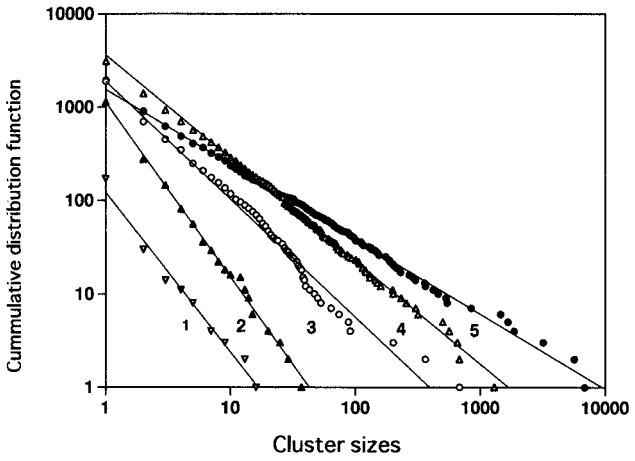

FIG. 2. Log-log plot of representative cumulative frequency distributions of LAA size. The five lung slices analyzed had LAA% values of 5.1 (1), 15.6 (2), 30.9 (3), 42.3 (4), and 60.4 (5). Eq. **1** then was fitted to the plots by linear regression. In these five cases, r has a value of 0.991, 0.997, 0.987, 0.998, and 0.998, respectively. The corresponding D values are 1.71, 1.87, 1.26, 1.10, and 0.64, respectively.

The values of the exponent D were obtained by linear regression in the log-log domain, and the correlation coefficients (r) were taken to indicate the goodness-of-fit of the power law. The values of D, r, and LAA% in three lung slices then were averaged for each subject. The mean ± SD values of r in the normal subjects and the COPD patients were 0.990 ± 0.006 and 0.988 ± 0.008, respectively, and were >0.949 in all subjects. There was no significant difference in the r values between the two groups, nor was there a relationship between r and LAA%. The values of D varied widely in the COPD ≤ 30 group. Although the COPD ≤ 30 group and the normal subjects had similar LAA% (17.4 ± 7.5 versus 15.6 ± 8.0; not significant, ANOVA), the corresponding D values were significantly smaller in the COPD patients (1.32 ± 0.26 versus 1.68 ± 0.40; $P < 0.0001$, ANOVA) (e.g., ≈3 vs. 1.7 in Fig. 1 *C* and *D*). In the COPD > 30 group, D was confined to a smaller and narrower range with a clear negative relationship between D and LAA% (Fig. 3). The correlation between LAA% and D was 0.904 including only COPD subjects, and it was 0.861 including all subjects.

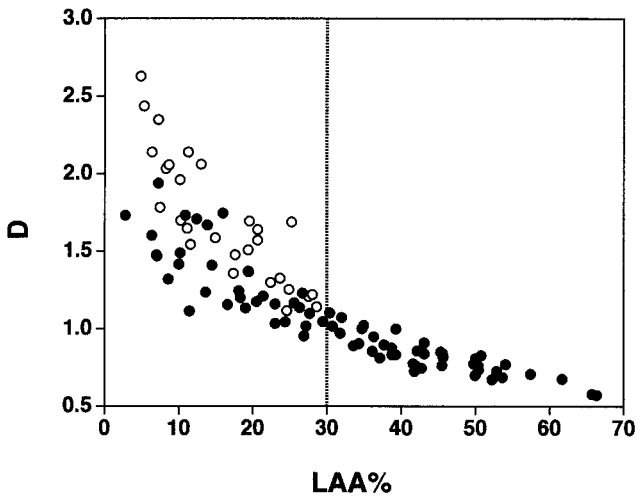

FIG. 3. Relationship between LAA% and D. Open and closed circles represent normal subjects and COPD patients, respectively. The LAA% in the normal subjects were all <30 (dotted lines).

In our COPD patients, the LAA% was significantly greater in the upper lung slice than in the middle slice (36.5 ± 21.2 versus 29.6 ± 17.51; $P < 0.05$, ANOVA), which suggests that most of the emphysematous lesions were of the centrilobular type (19). The histological characteristic of centrilobular emphysema is that the central portion of the lobule unit is involved during the early stage of the disease whereas the paraseptal tissue is kept intact. This suggests that the early development of centrilobular emphysema is spatially restricted by the bronchial and arterial tree structures.

Factors Influencing the Size Distribution of LAA Clusters

Lung CT images acquired *in vivo* are subject to various sources of artifact, such as the chest wall, the beating heart, pulsatile blood flow, changes in lung volume, and possible gas trapping. In the present study, the subjects were asked to hold their breath after a deep inspiration. Gevenois *et al.* (20) reported that quantitative characterization of macroscopic and microscopic emphysema from expiratory CT is not as accurate as from inspiratory CT. They speculated that abnormalities in the expiratory CT are more reflective of air trapping than of a real reduction in terminal airspace volume. Thus, our inspiratory CT is more suitable for the measurement of LAA distributions. There is a possibility that our observed decrease in D was not caused by the emphysematous changes in our COPD patients but rather by air trapping attributable to airway obstruction. This possibility is not likely, however, because the CT scanning was performed after a deep inspiration, and neither LAA% nor D correlated with FEV1/FVC in both normal and COPD subjects (Table 1).

To evaluate the influence of additional factors (e.g., presence of the chest wall, beating heart, etc.) on the LAA cluster distributions, we compared the CT images of several lung lobes *in situ* in patients with lung cancer to images of the same lobes obtained *in vitro* after their surgical removal, as follows. First, we selected four patients with normal lung function and four additional patients with COPD whose tumor sizes were <3 cm. The *in situ* CT images were obtained less than a month before the operation under the same conditions as in the present study. Images were obtained every 5 mm from lung apex to base. We chose three positions along the apical–basal axis for analysis. These positions were separated from each other by >3 cm, they were at least 0.5 cm from the tumor, and they contained only a single lobe. The mean LAA% and D from the three consecutive slices spanning each region then were calculated. Next, the lobes were carefully excised so that only a minimum amount of blood was lost and, within 20 minutes after excision, the lobes were inflated with a translobar pressure of 20 hPa. The inflated lobe was adjusted until its configuration was similar to that *in situ*, and the CT images were obtained immediately, again with a slice separation of 5 mm. We then selected three regions from the slices that matched the regions analyzed in the images obtained *in situ*. In each region, the threshold of LAA was established so that the difference between *in situ* and excised lung LAA% was <1%. Next, the mean values of LAA% and D were calculated from

Table 1. Correlation coefficients between CT and lung function parameters

	Normal	COPD ≤ 30	COPD > 30
n	30	31	42
LAA% vs. DLCO/VA	−0.203	−0.276	−0.362*
D vs. DLCO/VA	0.422*	0.407*	0.42*
LAA% vs. FEV1/FVC	0.174	−0.190	0.279
D vs. FEV1/FVC	−0.0060	0.312	0.203

COPD ≤ 30 and COPD > 30 represent those COPD patients whose LAA% was ≤30% and >30%, respectively.
*$P < 0.05$ (Fisher's Z transform)

the three consecutive slices spanning each region. Fig. 4 shows that the relationship between LAA% and D is similar to that in Fig. 3 for both the *in situ* and the *in vitro* lobes. The difference between the *in situ* and *in vitro* D values was 0.0751 ± 0.0520. The inset in Fig. 4 shows a very strong correlation between the *in situ* and *in vitro* D values ($r = 0.953$), with the slope of the regression line being not significantly different from unity. We thus conclude that D is not influenced by *in situ* artifacts and hence can be used to characterize the distribution of LAA clusters in both normal subjects and COPD patients.

Next, we evaluated the sensitivities of LAA% and D to changes in lung volume by using five normal subjects. The subjects held their breath at maximum inspiratory capacity, and three CT slices were scanned (top, middle, and bottom of the lung). They then were asked to expire 300 ml of air and to hold their breath again, and three more slices from similar positions were scanned. LAA% and D changed from 20.6 ± 5.2 to 18.3 ± 6.1 and from 1.56 ± 0.32 to 1.71 ± 0.34, respectively. These are changes in LAA% and D of 11.2% and 9.6%, respectively, which suggests that variability in lung volume among subjects cannot explain the large variability in D ($\approx$30%) that we found in normal subjects (Fig. 3).

The reproducibilities of LAA% and D were evaluated in five normal subjects and five COPD patients. Two separate CT scans were obtained 2 weeks apart, and the mean LAA% and D of three corresponding slices were compared. The mean $\pm$ SD of LAA% obtained from the first scan in the normal and COPD subjects were 16.27 ± 6.06 and 36.04 ± 12.36, respectively. The corresponding D values from the first scan were 1.781 ± 0.426 and 0.822 ± 0.293, respectively. The difference between the values of LAA% on the two occasions was 7.48 ± 2.60% in the normal subjects and 5.42 ± 3.25% in the COPD patients. The difference between the D values on the two occasions was 4.88 ± 1.85 and 4.58 ± 1.64% in the normal and COPD subjects, respectively. Thus, again, the good reproducibility of D (<5%) in repeated CT scans cannot account for the large variability of D ($\approx$30%) in normal subjects shown in Fig. 3. We conclude, therefore, that this variation reflects interindividual variation in lung structure.

Interpretation of the Size Distribution of LAA Clusters

We have so far established that the existence of a power law distribution of LAA cluster sizes and the numerical value of D are extremely robust and insensitive to a number of factors, including the chest wall, the beating heart, changes in lung volume, gas trapping, etc. The following questions then arise: What does the power law size distribution reflect, and what is the significance of the numerical value of D? In an attempt to interpret the power law distribution of LAA clusters, we first note that power laws abound in nature and are generally taken to reflect self-similar fractal structures of some kind (21–23). We suggest that the power law form of our LAA cumulative frequency distributions is yet another manifestation of this general phenomenon. Indeed, as mentioned earlier, the structure of the lung has distinct fractal aspects to it, such as the branching tree structure of the pulmonary airways and vasculature (24–27). In particular, the lung tissue is an object forming the alveolar surface that fills the three-dimensional space of the thorax and has been characterized as a fractal structure (9). Given that an LAA cluster is a two-dimensional slice of a macroscopic ensemble of specific alveolar regions, it seems inevitable that the LAAs will reflect the underlying structure of the tissue and so be fractal themselves.

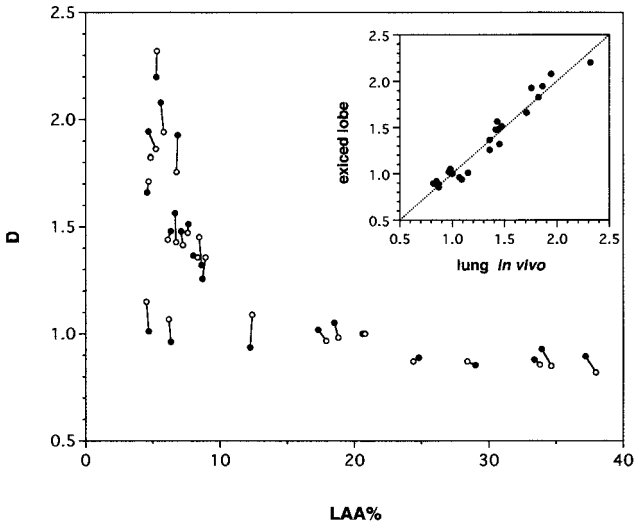

FIG. 4. Relationship between LAA% and D. Open and closed symbols represent data from *in vivo* lung and excised lobe, respectively. The inset shows the correlation between D obtained from *in vivo* CT images and from excised lobes. Dotted line is the line of identity.

Although D is not precisely equivalent to the fractal dimension d_f of the alveolar surface, it is nevertheless strongly related to d_f. When tissue density decreases, the space filling capacity of the lung tissue is reduced, and, hence, the value of d_f also must decrease. In a two-dimensional CT image, this would result in larger LAA clusters and, hence, a smaller D. Thus, differences in D between different subjects must reflect differences in the fractal structure of the lung tissue, where a smaller D is a consequence of a reduced fractal dimension d_f. Consequently, the value of D reflects the complexity of the terminal airspace geometry. The COPD subjects had a smaller D (and hence d_f) than normal subjects. If one assumes that emphysema involves the enlargement of existing LAAs, then this implies that large LAAs grow faster than small ones. One possible explanation for such an effect might be, for example, that a large LAA reflects the existence of more vigorous local pathology than a small LAA, so that the progression of the disease will be faster in the region of the larger LAA. Another possibility is that, as all of the LAAs grow in area, they tend to coalesce and so form some very large LAAs (e.g., see the green cluster in Fig. 1*B*) that will skew the distribution.

The critical value of LAA% = 30% can be used to differentiate between normal or mildly diseased lungs and very sick lungs. The value of D also can differentiate between these groups as $D < 1$ whenever LAA% > 30. However, the LAA% on its own is not sufficient to distinguish reliably between normal subjects and emphysematous patients in the early stage of the disease because the large variation in LAA% between individuals creates substantial overlap between the two groups. What is most significant from a practical point of view is our finding that D is less in COPD patients than in normal subjects, even when LAA% is similar (i.e., <30%) in the two groups (Fig. 1 *C* and *D*). Thus, the structures responsible for the establishment of LAAs in normal lungs appear to be significantly altered by the disease even in its early stages. Next, we seek the physical process that leads to a reduction in D while at the same time preserving LAA%.

Elastic Spring Network Model of Lung CT Images

To shed light on possible mechanisms by which structural alterations in the parenchyma might change the LAA% cluster distributions, we developed a two-dimensional elastic spring network model representing a slice of lung tissue. The model consisted of a 500×500 grid of nodes connected in a square lattice via Hookean springs having identical spring constants of 0.01, relaxed lengths of 0.5, and initial lengths of 1.0. The springs were thus prestressed to twice their relaxed lengths. The border nodes of the lattice were fixed, but the internal nodes were free to move. We mimicked an LAA in a CT image,

which represents a region of decreased alveolar tissue density, as follows. First, we randomly removed a node from the lattice by cutting the four springs connecting it to its neighbors. We then proceeded from this node in a random walk fashion to remove S additional adjoining nodes, each time cutting all springs that connected to them. This produced a cluster of $S + 1$ points that were removed from the lattice. We repeated this process NP times with a different randomly selected seed point, each time letting S vary uniformly between 0 and S_{max}. This produced a random distribution of clusters across the network. Finally, the equilibrium configuration of the remaining nodes was found by an iterative annealing type of scheme. The coordinates of each node were changed in small steps in the direction of the resultant force acting on it by its connecting springs until the elastic potential energy of the entire network was minimized. The node positions then were mapped onto a 500 × 500 pixel image, and the cluster size distribution and LAA% were determined in the same manner as for the CT images.

The LAA% of the model can be increased by increasing S_{max} and/or increasing NP. We chose S_{max} to be either 10 or 20 and varied NP between 1 and 16% of the total number of nodes. Three examples of the cluster distributions are shown in Fig. 5 together with their linear regressions. As NP is increased, the distribution becomes wider, covering almost four orders of magnitude when NP = 16%. The inset shows that the corresponding D values vary with LAA% in a quantitatively similar manner to that in Fig. 3.

We modeled the pathogenesis of emphysema by allowing those springs having tension greater than a certain threshold to break. This reflects the notion that the elastic fibers and eventually the alveolar walls will themselves break if they become overdistended. For the baseline case, the number of clusters (2,759) was chosen to give an LAA% of 11, similar to that of a normal subject. The resulting cluster structure of the model (Fig. 6*A*) is similar to that of the CT image of a normal subject (Fig. 1*C*) and has a power law region with an exponent of 2.5. We next identified the maximum spring tension in our model of the normal lung and then cut all springs whose tensions exceeded 80% of this maximum. This step eliminated <0.5% of the springs. The new equilibrium configuration of the network nodes was found, and the entire procedure was repeated three times. This process resulted in a total of 545

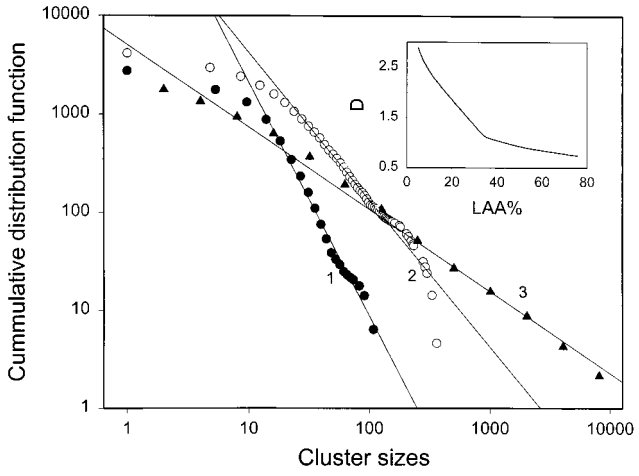

FIG. 5. Log-log plots of the cumulative distribution functions of the LAA clusters obtained from the spring network model. The cases 1, 2, and 3 have LAA% values of 12, 29, and 55%, respectively. The corresponding exponents D of the distributions are 2.2, 1.3, and 0.88, respectively. The inset shows the variation of D with LAA%. Small values of LAA% are generated by using S_{max} = 10, and medium and large values of LAA% are obtained with S_{max} = 20 whereas NP was increased from 1 to 16%.

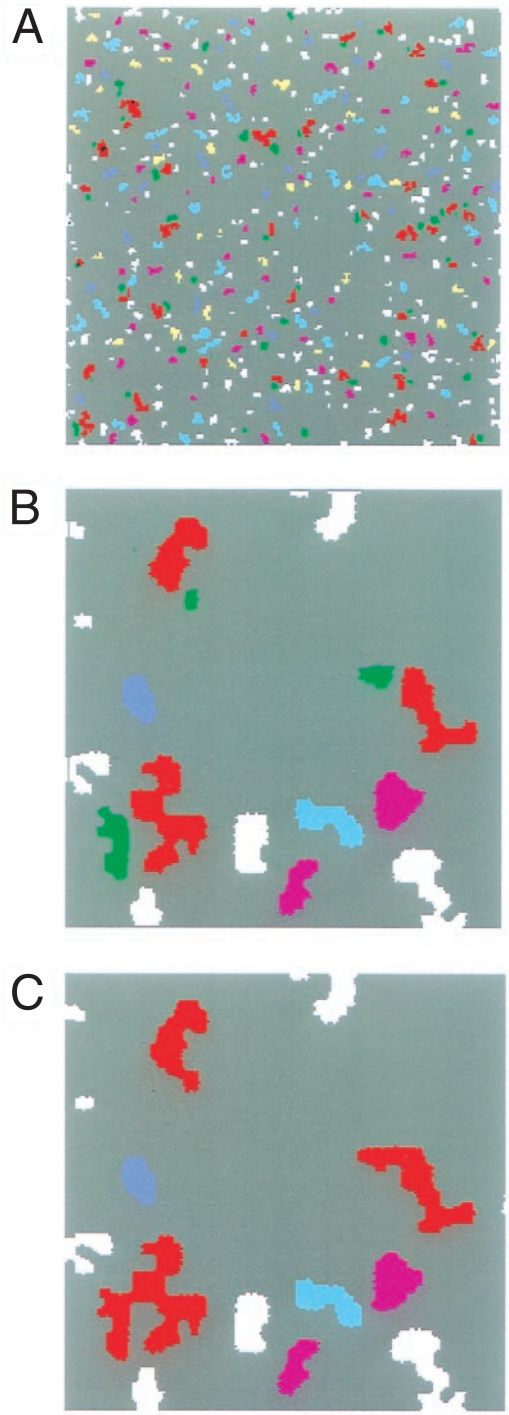

FIG. 6. Images obtained from simulations using a square lattice (500 × 500) of nodes connected by springs. The lattice constant is 1. The different colors represent LAA clusters in which several nodes have been removed from the network. (*A*) A 250 × 250 zoom in to the lattice. (*B*) Zoom into a small area (50 × 50) of the lattice in *A*. Notice that the three larger red clusters and the smaller neighboring green clusters are separated by tissue (gray). (*C*) The same network as in *B* but after 554 additional springs (whose tension was higher than 80% of the maximum tension) have been cut out of the 500 × 500 network. The tension in the walls separating the red and green clusters in *B* was high, and the alveolar walls broke. As a result, the green clusters are now part of the larger red clusters.

springs (of ≈500,000) being broken and caused LAA% to increase from 11 to 13%. Surprisingly, however, the total number of clusters decreased (to 2,565). This means that the cluster sizes must have increased, on average. A decrease in

cluster number and a simultaneous increase in LAA% (and hence mean cluster size) can occur if neighboring clusters tend to coalesce into a single larger cluster. This suggests that the narrow spring bridges separating such close clusters must have been under higher than average tension (causing them to break). Indeed, the image of the final network at the level of 500×500 nodes is visually indistinguishable from that in Fig. 6*A*. However, when we zoom in on the "normal" model image in Fig. 6*B*, we see several clusters that are separated by membranes of "tissue." These become cut, allowing the clusters to merge in Fig. 6C. Most striking, however, is that fact that this small ($<2\%$) increase in LAA% is accompanied by a much larger fractional decrease (24%) in *D* from 2.5 to 1.9.

The values of *D* calculated from the CT images seem to be equally sensitive to alterations in tissue structure that are not reflected in changes in LAA%. Table 1 shows that *D* was significantly correlated with DLCO/VA in all groups whereas LAA% showed a much weaker correlation with DLCO/VA that was significant only in the COPD $>$ 30 group. This suggests that the size of an LAA cluster is related to the local area of the blood–gas interface. That is, for a fixed LAA%, many small LAAs represent a greater surface area for gas exchange than a few larger LAAs. Thus, a decrease in *D* represents increased clustering of LAAs and consequently an enlargement in the terminal airspace area. This is in agreement with the interpretation that *D* is directly related to the fractal dimension characterizing the complexity of the alveolar tissue geometry. Thus, the enlargement in terminal airspace area as inferred from the LAA distributions appears to reflect the existence of early emphysema.

Conclusion

Although many anatomical and physiological attributes of the lung have been reported to have power law distributions, the clinical application of power law analysis to patients with pulmonary disease has not been previously explored. Our results show that power law analysis applied to the size distribution of LAA clusters is useful in revealing the pattern of progression of emphysema. Additionally, the exponent *D* of the power law distribution is a robust parameter, being sensitive only to changes in the fractal dimension of the alveolar tissue structure. Hence, *D* appears to be a powerful index for the detection of the terminal airspace enlargement that occurs in early emphysema.

The authors thank Mr. Ryuzo Tanaka, Mr. Hiroyuki Akazawa, Mr. Noboru Narai, and Ms. Miho Morimoto (Department of Radiology, Kyoto University Hospital, Kyoto) for their CT technical assistance and Dr. Sergey Buldyrev for helpful discussions. This study was funded by the Ministry of Education, Science and Culture of Japan and National Institutes of Health Grant HL 59215-01A1.

1. Goddard, P. R., Nicholson, E. M., Laszlo, F. & Watt, I. (1982) *Clin. Radiol.* **33,** 379–387.
2. Hayhurst, M. D., MacNee, W. & Wellenstein, D. E. (1984) *Lancet* **2,** 320–323.
3. Bergin, C., Müller, N. I., Nichols, D. M., Lillington, G., Hogg, J. C., Mullen, B., Grymaloski, M. R., Osborne, S. & Pare, P. D. (1986) *Am. Rev. Respir. Dis.* **133,** 541–546.
4. Gevenois P. A., Maertelaer, V., Vuyst, P., Zanen, J. & Yernault, J. C. (1995) *Am. J. Respir. Crit. Care Med.* **152,** 653–657.
5. Gelb, A. F., Scein, M., Kuei, J., Tashkin, D. P., Muller, N. L., Hogg, C., Epstein, J. D. & Zamel, N. (1993) *Am. Rev. Resp. Dis.* **147,** 1157–1161.
6. Uppaluri, R., Mitsa, T., Sonka, M., Hoffman, E. A. & McLennan, G. (1997) *Am. J. Respir. Crit. Care Med.* **156,** 248–254.
7. Shimizu, K., Johkoh, T., Ikezoe, J., Ichikado, K., Arisawa, J., Nakamura, H., Tamura, S. & Nagareda, T. (1997) *J. Comput. Assist. Tomogr.* **21,** 955–961.
8. Mandelbrot, B. B. (1983) *The Fractal Geometry of Nature* (Freeman, New York).
9. McNamee, J. E. (1991) *J. Appl. Physiol.* **71,** 1–8.
10. Weibel, E. R. (1991) *Am. J. Physiol.* **261,** L361–L369.
11. Horsfield, K. (1990) *J. Appl. Physiol.* **68,** 457–461.
12. Rigaut J. P. (1976) *J. Microsc. (Oxford)* **133,** 41–54.
13. Glenny, R. W. & Robertson H. T. (1990) *J. Appl. Physiol.* **69,** 532–545.
14. Glenny, R. W. & Robertson H. T. (1991) *J. Appl. Physiol.* **70,** 1024–1030.
15. Gilliard, N., Pappert, D. & Spragg R. G. (1995) *J. Appl. Physiol.* **78,** 862–866.
16. American Thoracic Society (1987) *Am. Rev. Respir. Dis.* **136,** 225–244.
17. Sakai, N., Mishima, M., Nishimura, N., Itoh H. & Kuno, K. (1994) *Chest* **106,** 1319–1325.
18. Dechman, G., Mishima, M. & Bates, J. H. T. (1994) *J. Appl. Physiol.* **76,** 1993–1998.
19. Thurlbeck, W. M. (1963) *Am. Rev. Respir. Dis.* **87,** 206–215.
20. Genenois, P. A., De Vuyst, P., Sy, M., Scillia, P., Chaminade, L., de Maertelaer, V., Zanen, J. & Yernault, J. C. (1996) *Radiology* **199,** 825–829.
21. Suki, B., Barabasi, A. L. & Hantos, Z. (1994) *Nature (London)* **368,** 615–618.
22. Vicsek, T. (1989) *Fractal Growth Phenomena* (World Scientific, Singapore).
23. Bates, J. H. T., Maksym, G. N., Navajas, D. & Suki, B. (1994) *Ann. Biomed. Eng.* **22,** 674–681.
24. Horsfield, K. & Thurlbeck, A. (1981) *Bull. Math. Biol.* **43,** 681–691.
25. Horsfield, K. & Woldenberg, M. J. (1989) *Anat. Rec.* **223,** 245–251.
26. Murray, C. D. (1926) *Proc. Natl. Acad. Sci. USA* **12,** 207–214.
27. Kitaoka H. & Suki B. (1997) *J. Appl. Physiol.* **82,** 968–976.